

AD-A176 248

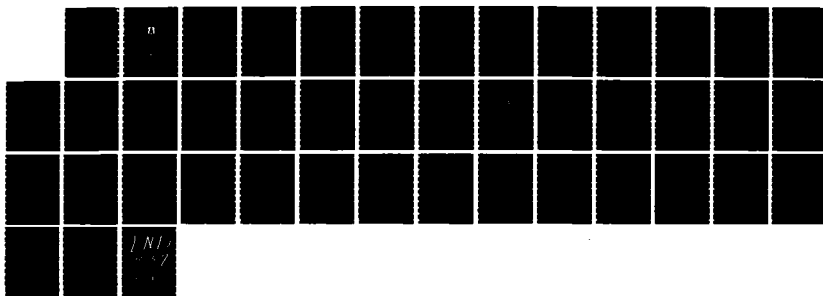
ACTA MECHANICA SINICA (SELECTED ARTICLES)(U) FOREIGN  
TECHNOLOGY DIV WRIGHT-PATTERSON AFB OH  
L BINGQIU ET AL 06 JAN 87 FTD-ID(RS)T-1152-86

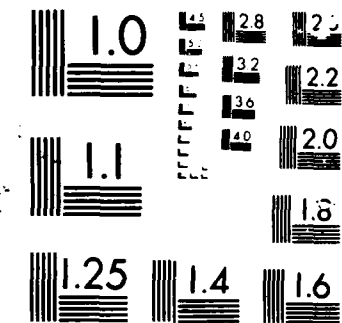
1/1

UNCLASSIFIED

F/G 28/4

NL





AD-A176 240

FTD-ID(RS)T-1152-86

(2)

## FOREIGN TECHNOLOGY DIVISION



ACTA MECHANICA SINICA  
(Selected Articles)

FILE COPY  
JMS



STIC  
SELECTED  
JAN 30 1987  
D  
E

Approved for public release;  
Distribution unlimited.



87 1 1

## **HUMAN TRANSLATION**

FTD-ID(RS)T-1152-86

6 January 1987

MICROFICHE NR: FTD-87-C-000040

ACTA MECHANICA SINICA (Selected Articles)

English pages: 37

Source: Lixue Xuebao, Vol. 18, Nr. 3, May 1986,  
pp. 200-207; 215-225

Country of origin: China

Translated by: FLS, INC.

F33657-85-D-2079

Requester: FTD/TQTA

Approved for public release; Distribution unlimited.

THIS TRANSLATION IS A RENDITION OF THE ORIGINAL FOREIGN TEXT WITHOUT ANY ANALYTICAL OR EDITORIAL COMMENT. STATEMENTS OR THEORIES ADVOCATED OR IMPLIED ARE THOSE OF THE SOURCE AND DO NOT NECESSARILY REFLECT THE POSITION OR OPINION OF THE FOREIGN TECHNOLOGY DIVISION.

PREPARED BY:

TRANSLATION DIVISION  
FOREIGN TECHNOLOGY DIVISION  
WPAFB, OHIO.

## GRAPHICS DISCLAIMER

All figures, graphics, tables, equations, etc. merged into this translation were extracted from the best quality copy available.

Accession For	
RTIG - GRANT	<input checked="" type="checkbox"/>
RTIG - TAN	<input type="checkbox"/>
University Card	<input type="checkbox"/>
3. Title/Section	
4. Primary Distribution	
5. Alternative Codes	
6. Date Due	
7. Signature	



A-1

TABLE OF CONTENTS

1. An Investigation of the Compressible Viscous Separated Vortex Over the Wing's Leading Edge, by Lin Bingqiu .....	1
2. A Discussion on the Principle of Flow-Velocity and Flow-Pattern Measurements Using Laser Spectral Lines, by Gao Zhi .....	17

# AN INVESTIGATION OF THE COMPRESSIBLE VISCOUS SEPARATED VORTEX OVER THE WING LEADING EDGE

Lin Bingqin

(Beijing Institute of Aerodynamics)

## Abstract

Based on the Navier-Stokes equations, the compressible viscous vortex equation describing the separated vortex of an aircraft is derived and a numerical method for solving this equation is developed. It can be used to subsonic, transonic and supersonic vortex flows. The breakdown condition of the compressible separated vortex is derived and used to compute the breakdown place. A series of interesting features about the effects of various parameters such as compressibility etc. on separated vortex motion are obtained and analysed.

AN INVESTIGATION ON THE COMPRESSIBLE VISCOUS SEPARATED VORTEX OVER  
THE WING LEADING EDGE

Lin Bingqiu  
(Berjing Institute of Aerodynamics)

Received on Feb. 17, 1985. A revised version was received on  
August 29, 1985.

Based on the Navier-Stokes equations, the compressible viscous vortex equation for describing the separated vortex of an aircraft is derived and a numerical method suitable for subsonic, transonic and supersonic flows is given which can compute the characteristics of separated vortex or trailing vortex. The break-down condition of the compressible separated vortex is derived and used to compute the break-down point. A series of interesting features about the effects of various parameters such as compressibility, etc. on separated vortex motion are obtained and analyzed.

I. Preface

The incident angle adopted by recent winged aircraft is becoming larger and larger in order to more effectively utilize the vortex lift generated by separated vortex of the component. But along with it comes the interference between the vortex system, between separated vortex and component, and between aircraft and trailing vortex. and the future motion state of the vortex itself also has unpredictable factors occurring sometimes. Therefore, a detailed study of the motion laws of the vortex itself becomes

the first step. Up until now, there has been much research, both theoretical and experimental, done on this low speed, incompressible vortex. Brown<sup>[1]</sup>, Hall<sup>[2]</sup>, and Muirhead<sup>[3]</sup>, etc. have done much research on the compressible viscous vortex, but it is still far from sufficient.

The effects of compressibility on the vortex are extremely distinct. We must establish a computation method suitable for subsonic, transonic and supersonic flows and clearly understand the effects of various parameters as well as the breakdown features of the compressible vortex, etc. This is exactly the subject which this paper wants to solve.

### II. Motion Equation of the Separated Vortex

We assume the vortex is laminar and symmetrical and can be described by N-S equations using cylindrical coordinates. The coordinates system  $x$ ,  $r$ ,  $\theta$  correspond to component velocities  $u$ ,  $v$ ,  $w$ . The external flow (or external flow field) of the vortex can be described by compressible, nonviscous, isentropic flow. Assuming the vortex is very slender, let  $\epsilon$  be the local slender ratio of vortex, and  $\epsilon$  is first-order small quantity. Based on quantity-net analysis,  $v = \epsilon u$  is derived from the continuity equation; we take  $w=0(u)$ . The coordinates and various physical quantities are written as normalized quantity-net forms according to this order of magnitude relations:  $\bar{r}=r/R_i$ ,  $\bar{x}=\epsilon x/R_i$ ,  $\bar{u}=u/u_i$ ,  $\bar{w}=w/u_i$ ,  $\bar{v}=v/\epsilon u_i$ ,  $\bar{p}=p/\rho_i u_i^2$ ,  $\bar{\rho}=\rho/\rho_i$ ,  $\bar{T}=c_p T/u_i^2$  and  $\bar{h}=h/u_i^2$ .

The bar above the nomenclatures denotes normalized quantity-net quantity.  $R_i$ ,  $\rho_i$  and  $u_i$  are initial radius, density and axial velocity at the outer edge of the vortex cross section, respectively, and here they are selected as reference quantities.  $p$ ,  $T$ ,  $h$  and  $c_p$  are pressure, temperature, enthalpy, and specific heat at constant pressure, respectively. Substitute the above normalized quantity-net quantities into the N-S equations, and take the reciprocal of Reynolds number  $R_e = \rho_i u_i R_i / \mu_i$  as a first-order small quantity, then omit the second-order small quantities in the equations to obtain vortex motion equations that describe the compressible viscous vortex:

$$\text{continuity: } \frac{\partial(r\rho u)}{\partial x} + \frac{\partial(r\rho v)}{\partial r} = 0 \quad (1)$$

$$\text{Axial Momentum: } \rho u \frac{\partial u}{\partial x} + \rho v \frac{\partial u}{\partial r} = - \frac{\partial p}{\partial x} + \frac{f}{r R_e} \frac{\partial u}{\partial r} + \frac{1}{R_e} \frac{\partial}{\partial r} \left( f \frac{\partial u}{\partial r} \right) \quad (2)$$

$$\text{Radial Momentum: } \frac{\rho w^2}{r} - \frac{\partial p}{\partial r} \quad (3)$$

$$\text{Rotational Momentum: } \rho u \frac{\partial w}{\partial x} + \rho v \frac{\partial w}{\partial r} + \frac{\rho w v}{r} = - \frac{2f}{r R_e} \left( \frac{\partial w}{\partial r} - \frac{w}{r} \right) + \frac{1}{R_e} \frac{\partial}{\partial r} \left[ f \left( \frac{\partial w}{\partial r} - \frac{w}{r} \right) \right] \quad (4)$$

$$\text{Energy Equation: } \rho u \frac{\partial T}{\partial x} + \rho v \frac{\partial T}{\partial r} = u \frac{\partial p}{\partial x} + v \frac{\partial p}{\partial r} + \frac{f}{R_e} \left[ \left( \frac{\partial u}{\partial r} \right)^2 + \left( \frac{\partial w}{\partial r} - \frac{w}{r} \right)^2 \right] + \frac{1}{r R_e P_r} \frac{\partial}{\partial r} \left( r f \frac{\partial T}{\partial r} \right) \quad (5)$$

where all quantities are normalized quantity-net quantities, and the bars above nomenclatures are omitted for the sake of convenient writing.  $P_r$  is the Prandtl number,  $f = \mu / \mu_i$ , the equation groups is a parabolic type, and solutions can be derived if initial and boundary values are known.

### III. Numerical Method of Vortex Equation

The method for solving partial differential equations (1)~(5) should be based on the mission of the problem. The net-grid method is suitable for computing vortex features in a certain section of the flow field, such as computing the features in the breakdown region. Even so, convergence is difficult to obtain at a slightly higher Reynolds number. It is not economical using this method to compute a slender trailing vortex either. In order for convenient theoretical investigation, we turned to the solution method similar to those adopted by Reference [4] and [5], and expanded it to solve for vortex motion taking compressibility into account.

1. Solve for the radial velocity  $v$  from equation (1),

$$v = -\frac{1}{r\rho} \int_0^r \frac{\partial(r\rho u)}{\partial x} dr,$$

and substitute into the  $v$ 's in equations (2), (4), (5). Then take the integral along the radial direction while noting the outer edge and core condition of the vortex

$$\left. \frac{\partial u}{\partial r} \right|_{r=R} - \left. \frac{\partial u}{\partial r} \right|_{r=\infty} = 0,$$

Differential and integral equations corresponding to (2), (4), (5) can be obtained:

$$\int_0^R \frac{\partial}{\partial x} [r\rho u(u - u_c)] dr + \frac{du_c}{dx} \int_0^R r\rho u dr = - \int_0^R r \frac{\partial p}{\partial x} dr \quad (6)$$

$$\int_0^R \frac{\partial}{\partial x} [r\rho u(c - C)] dr + \frac{dC}{dx} \int_0^R r\rho u dr = - \frac{2Cf_c}{Re} \quad (7)$$

$$\begin{aligned} & \int_0^R \frac{\partial}{\partial x} [r\rho u(T - T_c)] dr + \frac{dT_c}{dx} \int_0^R r\rho u dr \\ & - \int_0^R r u \frac{\partial p}{\partial x} dr - \int_0^R \left( \int_0^r \frac{\partial(r\rho u)}{\partial x} dr \right) \frac{u^2}{r} dr \\ & + \frac{1}{Re} \int_0^R f_r \left[ \left( \frac{\partial u}{\partial r} \right)^2 + \left( \frac{\partial u}{\partial r} - \frac{u}{r} \right)^2 \right] dr + \frac{Rf_c}{RePr} \frac{\partial T}{\partial r} \end{aligned}$$

where  $c = rw$  and  $C = R w_e$  are vortex internal and outer edge circulation parameters, respectively, and represent vortex intensity. The subscript "e" represents the vortex outer edge.

2. Expand the functions  $u$ ,  $w$ ,  $p$  inside the integral sign into polynomials:

$$u = \sum_{i=1}^{\infty} u_i \eta^i, \quad w = \sum_{i=1}^{\infty} w_i \eta^i, \quad p = \sum_{i=1}^{\infty} p_i \eta^i$$

where  $\eta = r/R$  and the coefficients in the expansion are determined by boundary conditions. If  $u$ ,  $w$ ,  $p$  are known, then  $\rho$  is obtained from (3) and  $T$  is obtained from the state equation  $T = \frac{r}{r-1} \frac{P}{\rho}$  in normalized quantity-net form.

At the outer edge of the vortex where  $r=R$ ,  $u=u_C$  and  $\frac{\partial u}{\partial r} = \frac{\partial^2 u}{\partial r^2} = 0$ ,  $w=C/R$ , and  $\frac{\partial c}{\partial r} = \frac{\partial^2 c}{\partial r^2} = 0$ ;  $p=p_e$  and  $\frac{\partial p}{\partial r} = \frac{p_e C^2}{R^3}$ .

At the vortex core where  $r=0$ ,  $u=u_0$ ,  $p=p_0$ ,  $w=0$  and  $\frac{\partial w}{\partial r}=w$ .

$w$  is called the vorticity parameter of core. Its relations with the vorticity of the vortex core is  $Q_0 = 2w/R$ ; and also from symmetrical feature

$$\frac{\partial p}{\partial r} = \frac{\partial u}{\partial r} = \frac{\partial \rho}{\partial r} = 0.$$

where  $\frac{\partial \rho}{\partial r} \Big|_{r=0} = 0$  is an additional condition for  $p$ . Each expansion has 5 boundary conditions; therefore, pentanomials are obtained as follows:

$$\left. \begin{aligned} u &= u_0(1 - 6\eta^2 + 8\eta^3 - 3\eta^4) + u_e(6\eta^2 - 8\eta^3 + 3\eta^4) \\ w &= \frac{C}{R} (10 - 15\eta + 6\eta^2)\eta^2 + w(1 - 3\eta + 3\eta^2 - \eta^3)\eta \\ p &= p_0 + p_1\eta^1 + p_2\eta^2 + p_3\eta^3 + p_4\eta^4 \end{aligned} \right\} \quad (9)$$

$$p_4 = - \frac{3b_1 \left[ \frac{\partial p}{\partial \eta} \Big|_{r=0} - 4(p_e - p_0) \right]}{2(3b_1 + b_2)},$$

$$p_1 = - \frac{b_2 \left[ \frac{\partial p}{\partial \eta} - 4(p_r - p_0) \right]}{3b_1 + b_2}$$

$$p_0 = (p_r - p_0) - (p_1 + p_2)$$

$$b_1 = \omega^2, b_2 = 20 \frac{C\omega}{R} - 6\omega^2, \frac{\partial p}{\partial \eta} = \alpha(C/R)^2$$

The subscript "0" denotes core vorticity.

3. In principle, substituting (9) into each differential and integral equation (6)-(8) and then taking the integral sequentially can simplify them into a group of differential equations. However, since the form of integral function is more complicated, it is extremely cumbersome to derive using an analytical method. For this reason, we adopted a more generalized method. Separate the first-order derivatives from the equations, then set the integral of various complicated forms as the coefficients of those first-order derivatives, and use a numerical method to compute these coefficients. In order to illustrate the derivation method, a term with the most representative form is selected for demonstration purposes, for instance:

$$\int_0^1 \eta^n \phi \left( \int_0^1 \eta^m \frac{\partial \phi}{\partial x} d\eta \right) d\eta.$$

where  $\phi = \phi(p_0(x), u_0(x), R(x), \omega(x), p_r(x), u_r(x), \epsilon(x))$

$\phi = \phi(p_0(x), u_0(x), R(x), \omega(x), p_r(x), u_r(x), C(x))$

Separate all the derivatives, then the above integral is written as:

$$F = \int_0^1 \eta^n \phi \left( \int_0^1 \eta^m \frac{\partial \phi}{\partial x} d\eta \right) d\eta = \sum_{i=1}^7 F_i Y_i$$

$$F_i = \int_0^1 \eta^n \phi \left( \int_0^1 \eta^m \frac{\partial \phi}{\partial Y_i} d\eta \right) d\eta \quad (i=1, 2, \dots, 7)$$

$Y_1 = p_o$ ,  $Y_2 = u_o$ ,  $Y_3 = w$ ,  $Y_4 = R$ ,  $Y_5 = p_c$ ,  $Y_6 = u_c$ ,  $Y_7 = C$ . In  $n$  and  $m < 0$ , an odd point will appear at the lower limit of the integral for the function under integration. But the odd point can be eliminated within the range of the problems we are solving.

Now three first-order, near-linear differential equations are obtained, yet there are four functions  $p_o$ ,  $u_o$ ,  $R$ ,  $w$  to be solved. Use a method similar to thos' in Reference [4] and [5] to make an equation (2) satisfy the boundary condition at the core and obtain a supplementary equation. Thus, a closed equation system is formed:

$$A \begin{bmatrix} p_o \\ u_o \\ R \\ \omega \end{bmatrix}' = B \begin{bmatrix} p_c \\ u_c \\ C \\ 0 \end{bmatrix} + \begin{bmatrix} f_1 \\ f_2 \\ f_3 \\ f_4 \end{bmatrix} \quad (10)$$

The apostrophe means to take the derivative once with respect to  $x$ , where

$$A = \begin{bmatrix} a_{11} + a_{31} & a_{12} & a_{17} + a_{37} & a_{15} + a_{35} \\ b_{11} & b_{12} & b_{17} & b_{15} \\ c_{11} - c_{31} + c_{41} & c_{12} + c_{42} & c_{17} + c_{37} - c_{47} & c_{15} - c_{35} + c_{45} \\ d_{11} & d_{12} & 0 & 0 \end{bmatrix}$$

$$B = \begin{bmatrix} -(a_{12} + a_{21}) & -(a_{11} + a_{21} + a_{31}) & a_{15} + a_{35} & 0 \\ -b_{12} & -b_{11} & -(b_{15} + b_{21}) & 0 \\ c_{12} - c_{21} - c_{42} & -(c_{11} + c_{21} - c_{31} + c_{41}) & c_{15} - c_{25} - c_{35} - c_{45} & 0 \\ 0 & 0 & 0 & 0 \end{bmatrix}$$

See appendix for the expressions of the aforementioned elements.

i. Equation (10) is a differential equation with functions of  $p_o$ ,  $u_o$ ,  $R$ ,  $w$  and with the  $x$ -axis coordinate as self-variance. Its right-hand side includes pressure  $p_c$  at the outer edge of

the vortex, axial velocity  $u_c$ , circulation parameter  $C$ , Reynolds number  $R_e$ , Prantdl number  $P_r$  and viscosity coefficient ratio  $f$ . It reflects physically the effects of nonuniform external flow, viscous diffusion and heat conduction on vortex motion. The initial conditions at the outer edge of the vortex are  $u_{c_i} = 1$  and  $R_i = 1$ . The initial pressure of external flow can also be expressed in the form of external flow initial Mach number  $M_{a_i}$ .  $M_{a_i} = [(1 - C_i^2) / \gamma p_{c_i}]^{1/2}$ . In the computations hereinafter,  $P_r$  and  $f$  are approximately taken as  $P_r = 1$  and  $f = (T/T_i)^{0.75}$ . When the initial values of external flow parameters and functions are given, then the Rung-Kutta method of fourth-order accuracy can be used to numerically solve equation (10). It is not limited by external flow  $M$  number.

#### IV. Analyses and Discussions of Calculated Results

##### 1. Typical Internal Distribution Features

We selected a group of initial parameters and external flow parameters which correspond to stable motion of separated vortex, and the calculated results are as shown in Fig. 1. It displays the radial changing laws of various physical quantities on two cross sections of the vortex in supersonic external flow.

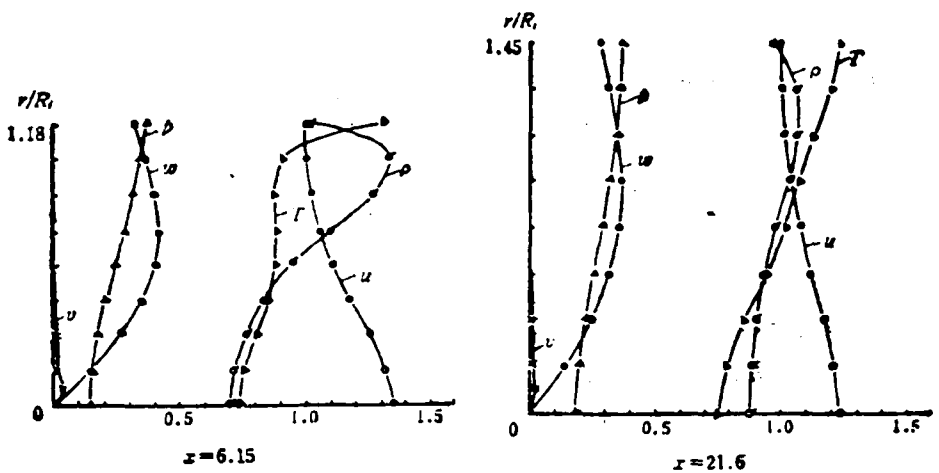


Fig. 1. Typical internal distribution features of supersonic separated vortex

$Ma_1 = 1.5$ ,  $p_{11} = 0.05$ ,  $\gamma_{\infty} = 1.5$ ,  $C_f = 0.4$ ,  $Re = 500$

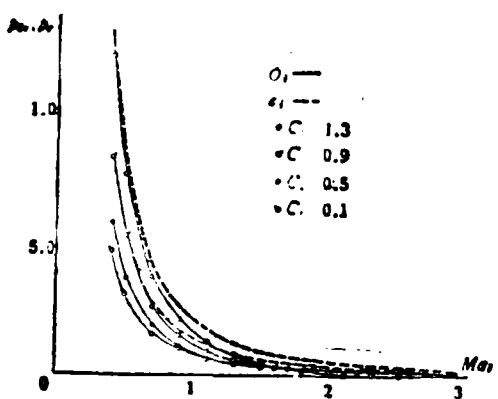


Fig. 2. Effects of compressibility on initial pressure at the vortex core

In the initial stage,  $x=1.65$ , and the changes in various physical quantities along the radial direction are greater. Further downstream, they then tend to stabilize and should become equal to those of the external flow. For every cross section, axial velocity  $u$ , near the vortex core is maximal, whereas density, pressure and temperature are

the opposite. The radial velocity  $v$  basically maintains its value as a second-order small quantity, which is consistent with the order of magnitude analysis. At the vortex core, axial velocity is in the deceleration process and gradually approaches 1. Pressure change is in the inversed pressure process. Rotational velocity  $w$  is similar to Berger distribution; it is 0 at the vortex core and after reaching maximum ( $\eta < 1$ ) as  $\eta$  increases, it approaches 0 at infinity. The vortex radius gradually expands and this is closely related to vortex core deceleration.

## 2. Compressibility Effect

The internal density of the vortex under high speed motion is variable. But  $\rho < 0$  must be maintained; it is the necessary physical condition for the vortex to be in existence. Substitute the expansion of  $p$  into (3) and let  $r=0$ , then the initial density at vortex core is:

$$\rho_i = \frac{3}{28} \left[ \frac{4(p_i - p_{\infty})}{C_i^2} - 1 \right],$$

Therefore, if satisfied

$$p_i - p_{\infty} > C_i^2/4 \quad (11)$$

or

$$p_{\infty} < \frac{1 + C_i^2}{\pi M a_i^2} - \frac{C_i^2}{4} \quad (12)$$

Thus,  $p_{\infty} > 0$  can be guaranteed. Equation (11) shows that only if a specific pressure difference is guaranteed can be existence of the vortex be maintained, and that at this time, the pressure at the vortex core must be lower than the external pressure. Equation (12) shows that the selected initial pressure and vortex intensity for the existence of the vortex are related to external flow Mach number. This relation is visually displayed by Fig. 2. Solid lines are the  $p_{\infty}$

curve at  $p_{o_i} = 0$  and constant  $C_i$ . Dotted lines are  $p_{c_i}$  curve at constant  $C_i$ . The region between solid lines and straight line  $p_{o_i} = 0$  (the abscissa) is the region where significant vortex core pressure  $p_{o_i}$  is selected, i.e., the region where the vortex can be formed. As  $Ma_i$  increases, said region becomes smaller. After  $Ma_i$  is greater than 1, this effect is more distinct. It stabilizes after  $Ma_i > 1.7$ . The larger  $C_i$  is, the smaller the region is. We have noted that when  $C_i$  is larger, and after  $Ma_i$  exceeds a certain limit, said region shrinks to zero. At this time, it is impossible to form the vortex. Moreover, under the condition of smaller  $C_i$  (as  $C_i = 0.1$  in the figure) and very large  $Ma_i$ , the pressure difference between the inside and outside of the vortex is almost negligible. At this time, it is meaningless to generate lift using separated vortex. In experiments, the measurements of pressure distribution for a slender cone-shaped lift body have shown<sup>[6]</sup> that the pressure peak on the surface trailing the wind becomes level as the supersonic Ma number increases, which means the disappearance of the effects of separated vortex.

### 3. Breakdown Phenomenon of Compressible Vortex

We assumed that there is a stationary point at the vortex core, and the origin of coordinates was set at the stationary point with positive direction of x-axis pointing downstream. Each physical quantity is expanded near the x-axis of the stationary point:

$$\left. \begin{aligned} u &= u_0(x) + u_1(x)r^1 + \dots, \quad v = v_1(x), + v_2(x)r^2 + \dots \\ w &= w_1(x)r + w_2(x)r^2 + \dots, \quad p = p_0(x) + p_1(x)r^2 + \dots \\ \rho &= \rho_0(x) + \rho_1(x)r^2 + \dots \end{aligned} \right\} \quad (13)$$

Substituting into the N-S equations and taking  $1/Re$  as higher than second-order small quantity, then the following is obtained:

$$\rho_0 u'_0 + 2\rho_0 v_1 = 0 \quad (14)$$

$$p'_0 + \rho_0 u_0 u'_0 = 0 \quad (15)$$

$$u_0 w'_0 + 2v_1 w_1 = 0 \quad (16)$$

From (14) and (15) to obtain, respectively

$$v_1 = -\frac{1}{2} u'_0 \quad (17)$$

$$p'_0 = -\rho_0 (u'_0)^2 / 2 \quad (18)$$

Substitute (17) into (16) to obtain

$$u_0 = c_1 w_1 \quad (19)$$

where  $c_1$  is an integral constant. That axial velocity should have the following features near the stationary point are already known:

$$u'_0|_{r=0} < 0 \quad \text{or} \quad (u'_0)'|_{r=0} < 0, \quad u'_0|_{r=0+} < 0 \quad \text{or} \quad (u'_0)'|_{r=0+} > 0$$

Therefore, it can be observed from (18) that  $p'_0$  increases from upstream of the stationary point to the stationary point and pressure is inversed along the axis. Conversely, pressure changes along the stream from the stationary point to downstream, i.e., pressure is maximal at the stationary point. It can be derived from (19) that  $w_1$  is equal to zero at the stationary point and that in the upstream and downstream areas near the stationary point,  $w_1$  changes sign after passing the stationary point because  $u_0$  changes sign. This shows that at the stationary point the radial gradient of rotational velocity,  $\partial w / \partial r|_{r=0} = 0$ , or vorticity  $Q=0$  (or  $w=0$ ).

After the vortex passes the stationary point, the rotational velocity of vortex reverses direction. Equation (17) shows that the radial gradient of radial velocity,  $\frac{\partial v_1}{\partial r}|_{r=0} > 0$ . Therefore, there is a negative branch surface starting from the stationary point. The

flow departs from the vortex core with the stationary point as the separation point, and it is also the odd point. Its mathematical condition is concluded as:

$$u_0 = 0, \omega = \Omega, -\frac{\partial w}{\partial r} \Big|_{r=0} = 0, \frac{\partial v}{\partial r} \Big|_{r=0} > 0 \quad (20)$$

It is the axially symmetrical breakdown condition of the vortex. It is completely identical in form to that of the incompressible vortex [4].

A large amount of computation and experiments for subsonic and transonic vortex flow have shown that the breakdown point takes two forms due to the effects of compressibility. One is the sudden change. Immediately upstream of the breakdown point, various physical quantities gradually change. At the breakdown point, the realization condition (20) can be approached. Figure 3 shows the calculated results under uniform external flow and subsonic condition. Breakdown place  $x_{BD} = 10.2$ , and  $u_0$  and  $w$  approach zero.

We studied the effects of various parameters such as  $C_i$ ,  $u_{oi}$ ,  $Re$  and initial pressure difference  $\Delta p_i = p_{ci} - p_{oi}$  on the breakdown point of the vortex through a large amount of computations. Increasing  $C_i$ ,  $\Delta p_i$ , respectively or reducing  $u_{oi}$ ,  $Re$ , respectively, will promote breakdown of the vortex. Conversely, they will delay the occurrence of breakdown. These conclusions are completely identical to the results of the incompressible vortex [4].

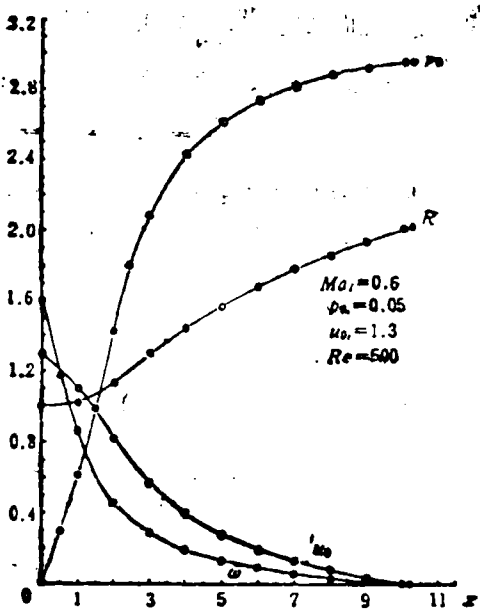


Fig. 3. Computation of the breakdown point of subsonic separated vortex

### Appendix

$$\begin{aligned}
 a_{ii} &= R^i \int_0^1 \eta \frac{\partial}{\partial Y_i} [\rho u(u - u_0)] d\eta \quad (i = 1, 2, \dots, 6) \\
 a_{ii} &= R^i \int_0^1 \eta \frac{\partial}{\partial R} [\rho u(u - u_0)] d\eta + 2R \int_0^1 \eta \rho u(u - u_0) d\eta \\
 a_{ii} &= R^i \int_0^1 \eta \rho u d\eta, \quad a_{ii} = R^i \int_0^1 \eta \frac{\partial \rho}{\partial Y_i} d\eta \quad (i = 1, 2, 4, 5, 6) \\
 a_{ii} &= R^i \int_0^1 \eta \frac{\partial \rho}{\partial R} d\eta + 2R \int_0^1 \eta \rho d\eta - RP_0 \\
 b_{ii} &= R^i \int_0^1 \eta \frac{\partial \rho u(c - C)}{\partial Y_i} d\eta \quad (i = 1, 2, \dots, 6) \\
 b_{ii} &= R^i \int_0^1 \eta \frac{\partial \rho u(c - C)}{\partial R} d\eta + 2R \int_0^1 \eta \rho u(c - C) d\eta, \quad b_{ii} = R^i \int_0^1 \eta u d\eta \\
 c_{ii} &= 3.5 R^i \int_0^1 \eta \frac{\partial}{\partial R} [u(\rho - 0.25 T_0 \rho)] d\eta + 7R \int_0^1 \eta u(P - 0.25 T_0 \rho) d\eta \\
 &\quad (i = 1, 2, \dots, 6) \\
 c_{ii} &= \frac{C^i}{R} \int_0^1 \rho u d\eta, \quad c_{ii} = R^i \int_0^1 \eta u d\eta, \quad (i = 1, 2, 4, 5, 6) \\
 c_{ii} &= R^i \int_0^1 \eta u \frac{\partial \rho}{\partial R} d\eta - R \int_0^1 \eta^2 u \frac{\partial \rho}{\partial \eta} d\eta \\
 c_{ii} &= R^i \int_0^1 \frac{u^2}{\eta} c_{ii} d\eta \quad (i = 1, 2, \dots, 7), \quad d_{ii} = 1, \quad d_{11} = \rho u_0 \\
 f_i &= \frac{1}{Re} \int_0^1 \eta f \left( \frac{\partial u}{\partial \eta} \right)^2 d\eta + \frac{1}{Re} \int_0^1 f \left( \frac{\partial u}{\partial \eta} - \frac{u}{\eta} \right)^2 d\eta + \frac{f}{RePr} \frac{\partial T}{\partial \eta} \\
 f_i &= \frac{24}{ReR^i} f_0 (u_0 - u_0)
 \end{aligned}$$

## REFERENCES

- [1] S.N. Brown, J.F. Mech, 22 (1965).
- [2] M.G. Hall, Progress in Aeronautical Science, 7 (1966).
- [3] V.J. Muirhead, AIAA Paper 73-106.
- [4] Lin Bingqiu, Acta Aeronautica Sinica, 3 (1981).
- [5] Lin Bingqiu, Acta Aeronautica Sinica, 2 (1983).
- [6] D. Köchemann, The Aerodynamic Design of Aircraft, Pergamon Press (1978).

A DISCUSSION ON THE PRINCIPLE OF FLOW-VELOCITY  
AND FLOW-PATTERN MEASUREMENTS USING  
LASER-SPECTRAL LINES  
高志

Gao Zhi

(Institute of Mechanics, Academia Sinica, Beijing)

Abstract

The principle of flow-velocity and flow-pattern measurements using Doppler-frequency-shifted absorption (or emission) spectral lines as well as Doppler-frequency-shifted and deformational non-saturation spectral line-shapes is discussed in this paper. For the case of gas flow with simultaneously inhomogeneously and homogeneously broadened line, the general expressions of non-saturation spectral line-shape and Doppler-frequency-shifted spectral line are presented. For the case of three representative gas flow with inhomogeneously broadened line, the concrete expressions of non-saturation spectral line-shapes and the qualitative and quantitative relationships among flow-velocity, flow-pattern, Doppler-frequency-shifted spectral line and deformational non-saturation spectral line-shape are also given.

A DISCUSSION ON THE PRINCIPLE OF FLOW-VELOCITY MEASUREMENTS USING  
LASER SPECTRAL LINES

Gao Zhi  
(Institute of Mechanics, Academia Sinica, Beijing)

Received on Dec. 25, 1984. A revised version was received on  
Nov. 1, 1985.

This paper investigates the problem of using frequency-shifted and deformational laser spectral lines to measure the gas macroscopic flow-velocity and flow-pattern. For the case of simultaneous effect by broadened Doppler lines and broadened pressure, the general expressions of nonsaturation spectral line-shapes and frequency-shifted relationship are obtained; for the case of three typical gas flow and primarily broadened Doppler lines, the specific expression of nonsaturation spectral line-shapes are obtained. The frequency-shift relationship and the qualitative and quantitative relationships among shifts and deformations of nonsaturation spectral line-shape, and gas macroscopic flow-velocity and macroscopic flow-pattern are also given.

I. Preface

The interaction phenomenon of gas flow and laser is somewhat different from the interaction phenomenon of gas and laser. The macroscopic flow of gas will cause the absorption (or emission) spectral lines to have frequency-shift due to the Doppler effect,

and deformation of nonsaturation spectral line-shapes will occur in addition to frequency-shift (saturation spectral line-shapes will certainly also have a similar situation occurring<sup>[2]</sup>). Frequency-shift, spectral line-shape shift and change in line width after deformation are all proportional to the flow-velocity component in the light-distance direction, thus flow-velocity can be measured according to laser spectral lines measurements<sup>[1]</sup>. Parameters such as gas flow density, temperature and gas composition naturally can also be obtained from laser spectral lines measurements. Using spectral lines frequency-shift to measure flow-velocity has the advantage of non-contact measurement; comparing with the laser Doppler velocity measurement method (LDV)<sup>[3]</sup>, it has the advantage of not requiring the addition of tracing particles in gas flow; therefore, there are no such problems as disruption of gas flow and whether particles can move with gas flow, nor are there limits on gas flow-velocity to be measured (or gas flow Mach number Ma) and gas flow acceleration. Spectral lines frequency-shift is proportional to the flow-velocity component in a light-distance direction. The larger the flow-velocity is, the more effective the said method is. Therefore, it has the unique advantage to transonic, supersonic flows and the measurements of their boundary layer flows. The shift and deformation situations of nonsaturation spectral line-shape are related to the gas macroscopic flow-pattern; therefore, said method is also possible to be used in diagnosing gas macroscopic flow-pattern.

Due to the distinguishability of spectra of different gas composition, isotopes and particles, as well as the development

in high resolution laser spectral technology, it is possible to more effectively utilize the laser spectral diagnosis method for parameter measurements of multi-composition gas mixture, isotope gas mixture and multi-phase flow, and meanwhile obtain parameter information such as flow-velocity, composition, density and temperature, etc.; said method can also be used in parameter measurements of various inhomogeneous gas flow media; for turbulent flow diagnosis, said method possesses a very large potential. Hence, it appears quite necessary to further study the principle of spectral velocity measurements, to conduct analyses and discussions on the situation of spectral lines frequency-shift as well as shifts and deformations in spectral line-shape.

## II. Nonsaturation Spectral Line-Shape of Gas Flow Medium

The spectral line-shape definition of spectrum is

$$g(\nu, \nu_0) = \frac{I(\nu)}{I} \quad (2.1)$$

$$I = \int_{-\infty}^{\infty} I(\nu) d\nu, \quad \int_{-\infty}^{\infty} g(\nu, \nu_0) d\nu = 1 \quad (2.2)$$

where  $\nu$  is frequency,  $\nu_0$  is spectral line center frequency;  $I(\nu)$  represents the distribution function of light intensity based on frequency,  $I$  is total light intensity. For the common gas situation in fluid dynamics, the contributions of Doppler broadening and pressure (homogeneous) broadening to spectral lines broadening are equally important. The nonsaturation spectral line-shapes for unmacroscopic fluid dynamic gas flow are:

$$g(\nu, \nu_0) = \int_{-\infty}^{\infty} g_D(\nu', \nu_0) g_H(\nu, \nu') d\nu' \quad (2.3)$$

where

$$g_D(v', v_0) = \frac{2}{\Delta v_D} \left( \frac{4\ln 2}{\pi} \right)^{1/2} \exp \left\{ - \left[ 4 \ln 2 \left( \frac{v' - v_0}{\Delta v_D} \right)^2 \right] \right\} \quad (2.4)$$

$$g_H(v, v') = \frac{\Delta v_H/2\pi}{(v - v')^2 + \left( \frac{\Delta v_H}{2} \right)^2} \quad (2.5)$$

$g_D(v', v_0)$  is the Gauss line-shape at center frequency of  $v_0$ ,  
 $g_H(v, v')$  is the Lorentz line-shape at center frequency of  $v'$ ;  
 $\Delta v_D$  and  $\Delta v_H$  are the full widths of Gauss and Lorentz spectral  
line-shapes at half-peak value, respectively, and are called line-  
shape width. At low gas pressure and predominantly Doppler broadening  
(i.e.,  $\Delta v_D \gg \Delta v_H$ ), take the approximation  $g_D(v', v_0) \approx g_D(v, v_0)$ , and  
(2.3) can be simplified as

$$g(v, v_0) = g_D(v, v_0) \quad (2.6)$$

At very high gas pressure and primarily homogeneous pressure broadening  
(i.e.,  $\Delta v_H \gg \Delta v_D$ ), take the approximation  $g_H(v, v') \approx g_H(v, v_0)$   
and (2.3) can be simplified as:

$$g(v, v_0) = g_H(v, v_0) \quad (2.7)$$

On the other hand, the nonsaturation and absorption (or emission)  
spectral line-shape of gas flow can be theoretically determined  
through a certain velocity distribution function of particles.  
This kind of particle velocity distribution function  $F(v')$  gives  
the probability for the particle to possess a displayed velocity  
between the range of  $v'$  and  $v' + dv'$  along the light-distance direction.  
For various homogeneous gas flow media, the displayed velocity  
 $v'$  can be expressed as the linear summation of the projection  
values  $v_i'$  ( $i=1, 2, 3$ ) on the light-distance direction of the three

coordinate components of particle thermal flow-velocity  $v_T$  and local average gas flow-velocity, i.e.,

$$v' = v_T + \sum_{i=1}^3 u_i \quad (2.8)$$

The particle velocity distribution function  $F(v')$  can be expressed as

$$F(v') = \prod_{i=1}^3 f_i(u_i) f_T(v_T) \quad (2.9)$$

where  $f_T(v_T)$  is the particle velocity distribution function corresponding to particle thermal flow;  $f_i(u_i)$  ( $i=1, 2, 3$ ) is the particle velocity distribution function corresponding to gas macroscopic flow;

$$f_T(v_T) \prod_{i=1}^3 f_i(u_i)$$

represents the combined probability for particles to be simultaneously in the thermal flow-velocity range between  $v_T$  and  $v_T - dv_T$ , and the projection values range between  $u_i$  and  $u_i - du_i$  ( $i=1, 2, 3$ ) on the light-distance direction of the coordinate components of gas macroscopic flow-velocity. The combined probability  $F(v')$  is naturally the probability for the particle to possess a displayed velocity between the range of  $v'$  and  $v' - dv'$ . These velocity distribution functions are defined as the unity integral, i.e.,

$$\int_{-\infty}^{\infty} f_T(v_T) dv_T = 1, \quad \int_{-\infty}^{\infty} f_i(u_i) du_i = \int_{-\infty}^{\infty} f_i(u_i) du_i = 1 \quad (2.10)$$

Also

$$\int_{-\infty}^{\infty} \int_{-\infty}^{\infty} \int_{-\infty}^{\infty} \prod_{i=1}^3 [f_i(u_i) du_i] = \int_{-\infty}^{\infty} \int_{-\infty}^{\infty} \int_{-\infty}^{\infty} [f_T(v_T) dv_T] = 1 \quad (2.11)$$

and

$$\int_{-\infty}^{\infty} \int_{-\infty}^{\infty} \int_{-\infty}^{\infty} f_T(v_T) \prod_{i=1}^3 [f_i(u_i) du_i] dv_T = 1 \quad (2.12)$$

$$\int_{-\infty}^{\infty} F(v') dv' = 1 \quad (2.13)$$

Here  $u_{i0}$  and  $u_{ic}$  are the two boundaries of  $u_i$  ( $i=1, 2, 3$ ). In order to solve the probability function  $F(v')$ , the following mathematical transformation is performed now

$$U_i = U_i(u_i, v_T) \quad (i = 1, 2, 3)$$

$$v' = \sum_{i=1}^3 u_i + v_T \quad (2.14)$$

where the specific function form of  $U_i(u_i, v_T)$  is related to the specific form of gas macroscopic flow, but the following equation is also true

$$\begin{aligned} 1 &= \iiint_{-\infty}^{\infty} f_T(v_T) \prod_{i=1}^3 [f_i(u_i) du_i] dv_T \\ &= \iiint_{-\infty}^{\infty} f_T(U_i, v') \prod_{i=1}^3 [f_i(U_i, v') dU_i] \frac{\partial(u_i, v_T)}{\partial(U_i, v')} dv' \end{aligned} \quad (2.15)$$

where

$$\frac{\partial(u_i, v_T)}{\partial(U_i, v')} = \begin{vmatrix} \frac{\partial u_1}{\partial U_1} & \frac{\partial u_1}{\partial U_2} & \frac{\partial u_1}{\partial U_3} & \frac{\partial v_T}{\partial U_1} \\ \frac{\partial u_2}{\partial U_1} & \frac{\partial u_2}{\partial U_2} & \frac{\partial u_2}{\partial U_3} & \frac{\partial v_T}{\partial U_2} \\ \frac{\partial u_3}{\partial U_1} & \frac{\partial u_3}{\partial U_2} & \frac{\partial u_3}{\partial U_3} & \frac{\partial v_T}{\partial U_3} \\ \frac{\partial u_1}{\partial v'} & \frac{\partial u_2}{\partial v'} & \frac{\partial u_3}{\partial v'} & \frac{\partial v_T}{\partial v'} \end{vmatrix} \quad (2.16)$$

For the case of a given specific flow field, the integral of (2.14) in the phase space  $(U_i, v')$  can be converted to the following form

$$\begin{aligned} &\iiint_{-\infty}^{\infty} f_T(U_i, v') \prod_{i=1}^3 [f_i(U_i, v') dU_i] \frac{\partial(u_i, v_T)}{\partial(U_i, v')} dv' \\ &= \int_{-\infty}^{\infty} \Phi(v', u_{i0}, u_{ic}) dv' = 1 \end{aligned} \quad (2.17)$$

Therefore,

$$F(v') = \Phi(v', u_{i0}, u_{ic}) \quad (2.18)$$

The displayed velocity  $v'$  of particle and its displayed frequency  $v'$  satisfy the Doppler relationship, and under first-order approximation of  $\frac{v'}{c} (\ll 1)$ , the Doppler relationship is

$$v' = \frac{c}{v_0} (v' - v_0) \quad (2.19)$$

Thus,

$$dv' = \frac{c}{v_0} dv' \quad (2.20)$$

where  $v_0$  is the resonant radiation frequency of particle at rest,  $c$  is the speed of light. It can be observed from (2.18)-(2.20) that the probability for the particle to be in its displayed frequency range from  $v'$  to  $v' + dv'$  in the frequency space is also the frequency distribution function of the particle, which is  $\frac{c}{v_0} \Phi(v' - v_0, u_{i0}, u_{ic})$  and satisfies the unity integral condition

$$\int_{-\infty}^{\infty} \frac{c}{v_0} \Phi(v' - v_0, u_{i0}, u_{ic}) dv' = 1 \quad (2.21)$$

For the general situation of simultaneous pressure broadening and Doppler broadening, the computation of nonsaturation absorption (or emission) spectral line-shapes must not only compute the contribution of the particle with radiation phase resonance at frequency  $v$  to the radiation at frequency  $v$ , but must also compute the contribution of the particle with displayed frequency  $v'(v' \neq v)$  to radiation at frequency  $v$  due to induced homogeneous broadening effect. Therefore, the general expression of nonsaturation spectral line-shape is

$$g_I(v, v_0) = \int_{-\infty}^{\infty} \frac{c}{v_0} \Phi(v' - v_0, u_{i0}, u_{ic}) g_H(v', v) dv' \quad (2.22)$$

For the spectral line-shape  $g(v, v_0)$  of spectral line-shape  $g_H(v, v_0)$

corresponding to gas unmacroscopic flow (refer to (2.3)), there are generally frequency-shift and deformation, broadening or narrowing of line width, decrease or increase in peak value. Since

$$\Delta v_D = \frac{2v_0}{c} a_p (\ln 2)^{1/2}, \quad a_p = \left( \frac{2kT}{m} \right)^{1/2} \quad (2.23)$$

where  $a_p$  is the most probable thermal flow-velocity,  $k$  is Boltzmann constant,  $m$  is mass of particle. When gas flow-velocity is of the magnitude of the speed of sound, the full width  $\Delta v_{\phi}$  at the half-peak value of the frequency distribution function  $\Phi(v' - v_0, u_{io}, u_{ic})$  is also of the magnitude of doppler line width  $\Delta v_D$ . Although the displayed velocity  $v'$  of the particle might be different from the thermal flow-velocity  $v_T$  of the particle (refer to (2.14)), the  $\sum_{i=1}^3 u_i$  contained in  $v'$  for gas microgroup is the same for all particles. Therefore, the following transformation can be performed

$$v' - v_0 = v'' - v_{of}, \quad v_0 - v_{of} = \frac{v_0}{c} \sum_{i=1}^3 u_i = \frac{1}{\lambda} \sum_{i=1}^3 u_i \quad (2.24)$$

where  $\lambda$  is laser wave length,  $v_{of}$  is the line-shape center frequency of nonsaturation spectral line-shapes of gas flow. (2.24) gives the shifts in location of spectral line-shapes peak value caused by gas macroscopic flow. The frequency-shift  $(v_{of} - v_0)$  is positive or negative based on whether the direction of  $\sum_{i=1}^3 u_i$  is concurrent or countercurrent to the laser propagation direction. The nonsaturation spectral line-shapes of gas flow is symmetrical or near-symmetrical to  $v = v_{of}$ . Considering (2.24) and also referring to the following text, (2.22) can be transformed to

$$g_I(v, v_{of}) = \int_{-\infty}^{\infty} \frac{c}{v_{of}} \Phi(v'', v_{of}) g_H(v'', v) dv'' \quad (2.25)$$

For the case of low gas flow pressure and gas flow spectral line-

shapes width  $\Delta v_p \gg \Delta v_H$ , the approximation of  $\Phi(v' - v_o, u_{io}, u_{ic}) = \Phi(v - v_o, u_{io}, u_{ic})$  and  $\Phi(v'', v_{of}) = \Phi(v, v_{of})$  can be adopted in performing the integral of (2.22) and (2.25). Therefore, from (2.22) and (2.25)

$$g_I(v, v_0) = \frac{c}{v_0} \Phi(v - v_0, u_{io}, u_{ic}) \quad (2.26)$$

$$g_I(v, v_{of}) = \frac{c}{v_{of}} \Phi(v, v_{of}) \quad (2.27)$$

Generally speaking,  $\frac{c}{v_{of}} \Phi(v, v_{of}) \approx g_D(v, v_{of})$ . For the case of very high gas flow pressure and  $\Delta v_H \gg \Delta v_p$ , the approximation of  $g_H(v', v) = g_H(v_o, v)$  and  $g_H(v'', v) = g_H(v_{of}, v)$  can be adopted in performing integral of (2.22) and (2.25). So, from (2.22) and (2.25)

$$g_I(v, v_0) = g_H(v, v_0) \quad (2.28)$$

$$g_I(v, v_{of}) = g_H(v, v_{of}) \quad (2.29)$$

(2.28) and (2.29) are consistent with (2.27), but they also contain a layer of new significance, i.e., under high gas flow pressure and  $\Delta v_H \gg \Delta v_p$ , the nonsaturation spectral line-shapes of gas flow is independent of gas flow conditions, and they are all homogeneous Lorentz line-shapes.

In addition, under the condition of  $u_i$  ( $i=1, 2, 3$ ) approaching 0, i.e., gas macroscopic flow, it is known from (2.14) and (2.15) that the particle frequency distribution function approaches Gauss line-shapes, i.e.,  $\frac{c}{v_0} \Phi(v - v_0, 0, 0) \rightarrow g_D(v, v_0)$ , and therefore, the nonsaturation spectral line-shapes equation (2.22) is simplified to spectral line-shapes equation (2.3).

### III. Derivation and Example

We will conduct specific discussions below on the three typical gas flows and the situation with predominantly nonhomogeneous Doppler broadening

#### 1. Shear Flow and One-Dimensional Homogeneous Flow

Assume the whole body (i.e., macroscopic) of a gas microgroup which is small macroscopically and large microscopically near a certain point in space moves along the x direction, and the magnitude of velocity is proportional to y (refer to Fig. 1), i.e.,

$$U_x = \frac{U_e - U_o}{l} y + U_o, \quad U_y = U_z = 0 \quad (3.1)$$

where l is the characteristic line degree of the gas microgroup. (3.1) also represents the flow along the x direction of the entire gas flow. The velocity gradient along the y direction is a constant shear flow, e.g., Couette flow<sup>[5]</sup>, etc. The special case of  $U_e = U_o$ ,  $U_x = U_o = \text{constant}$  in the shear flow equation (3.1) is a one-dimensional homogeneous flow. Assume the laser measurement is conducted along A and B directions (refer to Fig. 1); A direction is perpendicular to gas flow direction (i.e., x direction), and B direction is at an angle  $\theta$  with A direction. For B direction, the projection values of the three coordinate components of gas flow-velocity are, respectively

$$u_1 = U_x \sin \theta, \quad u_2 = u_3 = 0 \quad (3.2)$$

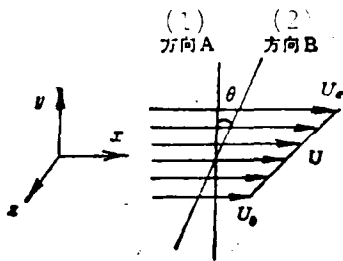


Fig. 1. Shear flow  
Key: (1) A direction; (2) B direction.

Considering the fact that gas flow density is constant and velocity distribution is linear distribution; therefore, the velocity distribution function  $f_i(u_i)$  is

$$f_i(u_i) = \begin{cases} \delta(u_i - U_s \sin \theta), & U_s - U_s = U_s \\ \frac{1}{(U_s - U_s) \sin \theta} & U_s > U_s \\ f_i(u_s) = \delta(0), & f_i(u_s) = \delta(0) \end{cases} \quad (3.3)$$

$\delta$  is a function of  $\delta$ . The following mathematical transformation is performed

$$U_1 = v_T - u_1, \quad U_2 = u_2, \quad U_3 = u_3, \quad v' = v_T + u_1 \quad (3.4)$$

Then

$$\begin{aligned} \frac{\partial(u_i, v_T)}{\partial(U_i, v')} &= -\frac{1}{2} \\ \iint \iint \iint f_T(v_T) \prod_{i=1}^3 [f_i(u_i) du_i] dv_T & \\ &= \int_{-\infty}^{\infty} \int_{v'+2U_s \sin \theta}^{\infty} \frac{1}{2a_p \sqrt{\pi}} \exp \left[ -\frac{(v' + U_s)^2}{4a_p^2} \right] f_i \left( \frac{v' - U_s}{2} \right) dU_i d\sigma' \\ &= \int_{-\infty}^{\infty} \frac{1}{2(U_s - U_s) \sin \theta} \left[ \operatorname{erf} \left( \frac{v' + U_s \sin \theta}{a_p} \right) \right. \\ &\quad \left. - \operatorname{erf} \left( \frac{v' + U_s \sin \theta}{a_p} \right) \right] dv' \end{aligned} \quad (3.5)$$

where  $\operatorname{erf}(x) = \frac{2}{\sqrt{\pi}} \int_0^x e^{-t^2} dt$  is the probability integral.  $f_T(v_T)$  is

assumed to be the Maxwell balanced distribution of a single velocity component when (3.5) is derived. Using (2.19) and (2.20), the nonsaturation spectral line-shapes of shear flow are obtained from (3.5)

$$g_1(\nu, \nu_0) = \frac{2(\ln 2)^{1/2}}{\Delta\nu_D} \frac{a_s}{2(U_e - U_0) \sin \theta} \left[ \operatorname{erf} \left( 2\sqrt{\ln 2} \frac{\nu - \nu_0}{\Delta\nu_D} + \frac{U_e \sin \theta}{a_s} \right) \right. \\ \left. - \operatorname{erf} \left( 2\sqrt{\ln 2} \frac{\nu - \nu_0}{\Delta\nu_D} + \frac{U_0 \sin \theta}{a_s} \right) \right] \quad (3.6)$$

When  $\theta=0$ , i.e., investigating along A direction, the nonsaturation spectral line-shape is regressed from (3.6) to

$$\frac{2}{\Delta\nu_D} \sqrt{\frac{\ln 2}{\pi}} \exp \left[ -\left( 4\ln 2 \right) \left( \frac{\nu - \nu_0}{\Delta\nu_D} \right)^2 \right] \quad (3.7)$$

This is the Gauss line-shape that coincides with the nonsaturation spectral line-shapes of gas macroscopic flow. For one-dimensional, homogeneous flow, i.e., when  $U_x = \text{constant}$  and  $U_e = U_0$ , (3.6) is regressed to

$$g_1(\nu, \nu_0) = \frac{2}{\Delta\nu_D} \sqrt{\frac{\ln 2}{\pi}} \exp \left[ -\left( 4\ln 2 \right) \left( \frac{\nu - \nu_0}{\Delta\nu_D} \right)^2 \right] \\ \nu_{sf} = \nu_0 - \Delta\nu_f, \quad \Delta\nu_f = \frac{U_e}{a_s} \frac{\Delta\nu_D}{2\sqrt{\ln 2}} \sin \theta \approx 0.6 Ma_e \Delta\nu_D \sin \theta \quad (3.8)$$

or

$$\Delta\nu_f = \frac{Ma_e}{\lambda} \sin \theta \quad (3.9)$$

where  $Ma_e$  is the gas flow Mach number. (3.8) and (3.9) show that: for one-dimensional homogeneous flow ( $U_e = U_0 = U_x$ ), the nonsaturation spectral line-shapes measured along B direction are still Gauss line-shapes, and said line-shapes have frequency-shift with respect to the Gauss line-shapes measured along A direction. The amount of frequency-shift  $\Delta\nu_f$  of the location of line-shapes peak value is given by (3.9). These conclusions are consistent with the analytical conclusions of Reference [1]. The analysis of Reference

[2] indicate: if the time required for the gas flow to pass through a laser light-beam cross section can be compared with molecular energy-level collision life (e.g., when light-beam width is 0.1 cm and flow-velocity perpendicular to light-beam is  $5 \times 10^2$  m/sec, the time for gas flow to pass through the light-beam cross section is only  $2 \times 10^{-6}$  sec), then the gain saturation rule of gas flow medium and saturation spectral line-shapes will all be different from the situation of gas unmacroscopic flow. However, the non-saturation gain of gas flow medium and nonsaturation spectral line-shapes are consistent with the situation of gas unmacroscopic flow; the aforementioned analyses reconfirm this conclusion and further show that: the nonsaturation spectral line-shapes measured leaning toward the gas flow direction can be obtained through frequency-shift changes of nonsaturation spectral line-shapes measured perpendicular to the gas flow direction. The amount of frequency-shift  $\Delta v_f$  of the location of spectral line-shapes peak value is given by (3.9).  $\Delta v_f$  is proportional to the product of flow-velocity,  $\Delta v_D$  and the sine of the angle between the two directions, and Fig. 2 gives the relationship of  $\Delta v_f/\Delta v_D$  with the change of gas flow Mach number  $Ma_e$ ;  $\Delta v_f$  is inversely proportional to wave length  $\lambda$ ; refer to equation (3.9). This is consistent with the relationship of single spectral line Doppler frequency-shift. Therefore, in the domain from the infrared to ultraviolet laser spectrum, a gas flow-velocity of 1 m/sec will cause a frequency-shift between 0.1 MHz and 10 MHz approximately.

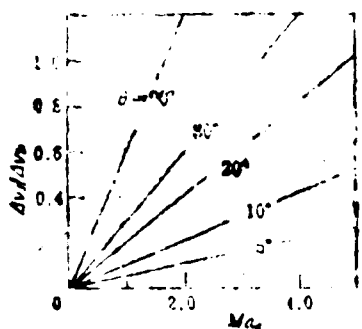


Fig. 2. Relationship between amount of frequency-shift and  $Ma_e$

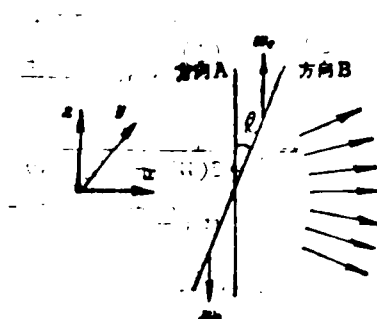


Fig. 3. Two-dimensional expansion flow  
Key: (1) A direction;  
(2) B direction.

For shear flow condition of  $U_e \neq U_o$ , equation (3.6) can be transformed to

$$g_1(\nu, \nu_0) = \frac{2\sqrt{\ln 2}}{\Delta \nu_D} \frac{a_p}{2(U_e - U_o) \sin \theta} \left[ \operatorname{erf} \left( 2\sqrt{\ln 2} \frac{\nu - (\nu_0 - \nu_f)}{\Delta \nu_D} \right) + \frac{U_e - U_o \sin \theta}{2a_p} \right] - \operatorname{erf} \left( 2\sqrt{\ln 2} \frac{\nu - (\nu_0 - \nu_f) - \frac{U_e - U_o \sin \theta}{2a_p}}{\Delta \nu_D} \right) \quad (3.10)$$

where

$$\nu_f = \frac{U_e + U_o}{2a_p} \frac{\Delta \nu_D}{2\sqrt{\ln 2}} \sin \theta \quad (3.11)$$

It can be observed from (3.10) and the following text that shear flow nonsaturation spectral line-shapes are equivalent to nonsaturation spectral line-shapes of two-dimensional symmetrical expansion flow.

## 2. Two-Dimensional Expansion Flow

In the domain of detection points, assume a flow-velocity component along axial direction ('x' direction):  $U_x \cong U_s$  (constant), flow-velocity component  $u$  along lateral direction ('y' direction):  $u =$

linearly from  $-w$  to  $w_e$ ; refer to Fig. 3; for the two detection directions, A direction is perpendicular to x-axis, B direction is at an angle  $\theta$  with A direction. The projection values of the three coordinate components of flow-velocity are

$$u_1 = U_e \sin \theta = U_e \sin \theta, u_2 = 0, u_3 = u \cos \theta$$

$$w = \frac{w_e - w_0}{l} z + w_0 \quad (3.12)$$

For homogeneous expansion flow, it can be assumed that within the velocity range of  $-w_0 \leq w \leq w_e$  the distribution probability of gas particles in the macroscopic flow-velocity space is constant, so the velocity distribution functions of particles are

$$f_1(u_1) = \delta(u_1 - U_e \sin \theta), f_2(u_2) = \delta(0)$$

$$f_3(u_3) = \begin{cases} \delta(0) & W_e = W_0 = 0 \\ \frac{1}{(W_e + W_0) \sin \theta} & |u_3| \leq \max(|W_e| \cos \theta, |W_0| \cos \theta) \\ 0 & |u_3| > \max(|W_e| \cos \theta, |W_0| \cos \theta) \end{cases} \quad (3.13)$$

Perform transformation

$$U_1 = u_1, U_2 = u_2, U_3 = v_T - u_1, v' = z + u_1 + u_3 \quad (3.14)$$

then

$$= \int_{-\infty}^{\infty} \int_{v' - U_e \sin \theta - 2W_e \cos \theta}^{v' + U_e \sin \theta + 2W_e \cos \theta} \frac{1}{2(W_e + W_0) \cos \theta} \frac{1}{a_p \sqrt{\pi}} \times \exp\left[-\frac{(v' + U_e \sin \theta + U_1)^2}{4a_p^2}\right] dU_1 d\sigma' \\ = \int_{-\infty}^{\infty} \frac{1}{2(W_e + W_0) \cos \theta} \left[ \text{erf}\left(\frac{v' + U_e \sin \theta + W_e \cos \theta}{a_p}\right) - \text{erf}\left(\frac{v' + U_e \sin \theta - W_e \cos \theta}{a_p}\right) \right] dv' \quad (3.15)$$

Therefore, the nonsaturation spectral line-shapes of expansion flow are

$$g_I(\nu, \nu_0) = \frac{2\sqrt{\ln 2}}{\Delta\nu_D} \frac{a_p}{2(W_0 + W_e) \cos\theta} \left[ \operatorname{erf} \left( 2\sqrt{\ln 2} \frac{\nu - \nu_{of}}{\Delta\nu_D} + \frac{W_e \cos\theta}{a_p} \right) - \operatorname{erf} \left( 2\sqrt{\ln 2} \frac{\nu - \nu_{of}}{\Delta\nu_D} - \frac{W_e \cos\theta}{a_p} \right) \right] \quad (3.16)$$

where  $\nu_{of} = \nu_0 - \Delta\nu_f$ , see equation (3.9). In equation (3.16), let  $\Delta\nu_f = 0$  and obtain the nonsaturation spectral line-shapes measured along A direction. So, the constant velocity macroscopic flow of gas along x direction will cause the nonsaturation spectral line-shapes measured in B direction to have a specific frequency-shift with respect to the spectral line-shapes in A direction. The amount of frequency-shift is consistent with the amount of line-shapes center frequency-shift  $\Delta\nu_f$  of gas unmacroscopic expansion flow (see (3.9)), and this indicates that gas with nonsaturation spectral line-shapes of complex macroscopic flow is the superposition of gas with spectral line-shapes of simple macroscopic flow. If gas flow expansion is weak,  $W_e/a_p \ll 1$ ,  $W_0/a_p \ll 1$ , then equation (3.16) is regressed to equation (3.8); if the effects of gas flow macroscopic expansion flow cannot be neglected, the expansion flow will make nonsaturation spectral line-shapes become non-Gauss line-shapes, and the spectral line-shape peak value decreases (expansion condition) or increases (convergent gas flow condition), line width broadens or narrows. The location of the spectral line-shape peak value obtained from (3.16) is

$$\nu_m = \nu_0 - \Delta\nu_f + \frac{\Delta\nu_D}{4\sqrt{\ln 2}} \frac{\cos\theta}{a_p} (W_0 - W_e) \quad (3.17)$$

Therefore, the amount of frequency-shift  $\Delta\nu_e$  of asymmetrical expansion spectral line-shape peak value location with respect to symmetrical expansion ( $W_e = W_0$ ) spectral line-shape peak value location is

$$\Delta\nu_c = \frac{\Delta\nu_D}{4\sqrt{\ln 2}} \frac{\cos\theta}{a_s} (W_0 - W_c) \quad (3.18)$$

Substitute (3.18) into (3.16) to obtain the magnitude of spectral line-shape peak value

$$\begin{aligned} \max g_i(\nu, \nu_0) &= g_i(\nu_m, \nu_0) \\ &= \frac{2\sqrt{\ln 2}}{\Delta\nu_D} \frac{a_s}{(W_0 + W_c)\cos\theta} \operatorname{erf} \left[ \frac{\cos\theta}{2a_s} (W_0 + W_c) \right] \end{aligned} \quad (3.19)$$

The half width  $\Delta\nu_D^* = (v_D - v_{0f})$  at the half peak value of spectral line-shape is obtained from the relationship below;  $v_D$  is the frequency at half peak value location,  $v_D = v_{0f} + \Delta\nu_D^*$ ,

$$\begin{aligned} \operatorname{erf} \left( 2\sqrt{\ln 2} \frac{\Delta\nu_D^*}{\Delta\nu_D} + \frac{W_c \cos\theta}{a_s} \right) &= \operatorname{erf} \left( 2\sqrt{\ln 2} \frac{\Delta\nu_D^*}{\Delta\nu_D} - \frac{W_0 \cos\theta}{a_s} \right) \\ &= \operatorname{erf} \left[ \frac{\cos\theta}{2a_s} (W_0 + W_c) \right] \end{aligned} \quad (3.20)$$

We better make some generalized mathematical discussions on expansion flow nonsaturation spectral line-shapes, let

$$W_s = aW_c, \quad X = 2\sqrt{\ln 2} \frac{\nu - \nu_{0f}}{\Delta\nu_D}, \quad Y = \frac{W_c \cos\theta}{a_s} \quad (3.21)$$

$$\begin{aligned} g(X, Y) &= \frac{\Delta\nu_D \sqrt{\pi}}{2\sqrt{\ln 2}} g_i(\nu, \nu_0) \\ &= \frac{\sqrt{\pi}}{2Y} [\operatorname{erf}(X + Y) - \operatorname{erf}(X - aY)] \end{aligned} \quad (3.22)$$

Perform mathematical transformation

$$X' + Y' = X + Y, \quad X' - Y' = X - aY \quad (3.23)$$

Then

$$\begin{aligned} g(X, Y) &= g(X', Y') = \frac{\sqrt{\pi}}{2Y'} [\operatorname{erf}(X' + Y') - \operatorname{erf}(X' - Y')] \\ &= \frac{\sqrt{\pi}}{2Y'} \frac{X' - aY'}{1 + a} \quad (3.24) \end{aligned}$$

$$\max g(X, Y) = \max g(X', Y') = \frac{\sqrt{\pi}}{2Y'} \operatorname{erf}(Y') \quad (3.25)$$

Therefore, all the nonsaturation spectral line-shapes of expansion

flow can be obtained from the spectral line-shapes of expansion flow through the near-jet transformation equation (3.23). From (3.10) it is also known that shear flow spectral line-shapes are also equally equivalent to the spectral line-shapes of a symmetrical expansion flow. Figure 4 gives several spectral line-shapes, where curve 1 is a Gauss line-shape; curve 2 is a symmetrical expansion flow ( $W_o = W_e$ ) spectral line-shape and curves 3 and 4 are asymmetric expansion flow spectral line-shapes. Figure 5 gives the relationship curves of nonsaturation spectral line-shapes peak values with the changes in  $W_e \cos\theta/a_p$ . Peak values drop monotonously as  $W_e \cos\theta/a_p$  increases. See Fig. 6 for the relationship of line width nonsaturation spectral line-shapes with the changes in  $W_e \cos\theta/a_p$ . The increase in line width is comparable to  $\Delta v_D$ ; therefore, the expansion flow-pattern and magnitude of expansion velocity can be measured according to the changes in line-shapes and line width.

In the relationship equation (3.16) of expansion flow spectral line-shapes, if we let  $W_e = W_o$  and use  $(U_e - U_o) \sin\theta/2$  to substitute  $W_e \cos\theta$ , then equation (3.16) is transformed into shear flow spectral line-shapes equation (3.10). Hence, the analytical conclusions and those relational curves of symmetrical expansion flow in Fig. 4 through Fig. 6 are equally suitable for shear flow. Here we emphasize again that: for emission spectral line-shapes, the flow indicated in the above analyses is the flow in the neighboring region of the radiation emission point (i.e., measurement point); therefore, it is distinguishable in space and can realize simultaneous measurement of multiple points. For absorption spectral line-shapes, the flow

indicated in the above analyses is the average flow along the light-distance direction and within light-distance length. If the flow-pattern along the light-distance direction and within the light-distance length is singular and the magnitude of the flow-velocity component along the light-distance direction remains constant, then those formulae given by this paper are accurately suitable; if the flow-pattern is not singular and the magnitude of the velocity component varies, then the formulae of this paper give the relationships of spectral line-shapes of average flow along the light-distance direction and the light-distance length.

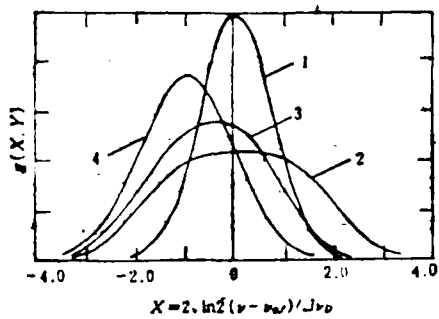


Fig. 4. Non-saturation spectral line-shapes ( $Y = W_s \cos \theta / a_s$ )  
 1— $W_s = W_o = 0$ ; 2— $W_s = W_o, Y = 2$   
 3— $W_s = 2W_o, Y = 2$ ; 4— $W_s = 0, Y = 2$

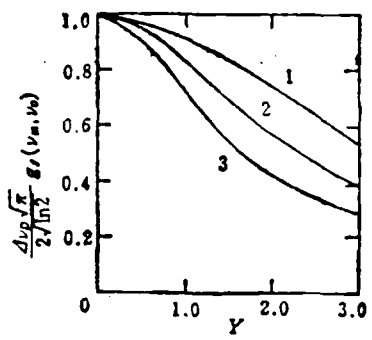


Fig. 5. Changes of spectral line-shape indices with  $Y = \frac{W_s \cos \theta}{a_s}$   
 1— $W_s = W_o$ ; 2— $W_s = 2W_o$   
 3— $W_s = 0$

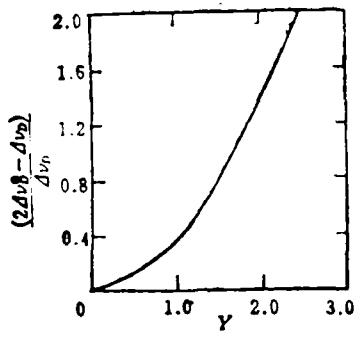


Fig. 6. Changes of the ratio of non-saturation and saturation spectral line-shapes with  
 $Y = \frac{W_s \cos \theta}{a_s}$  ( $W_s = W_o$ )

## Closing Remarks

Spectral lines and nonsaturation spectral line-shpaes will have frequency-shift, deformation and change in line width due to macroscopic flow of gas; within the domain from the infrared to ultraviolet laser spectrum, a gas macroscopic flow-velocity of 1 m/sec will cause frequency-shift and line width change between  $0.1 \text{ MHz}$  and  $10 \text{ MHz}$ , and these frequency-shifts and changes, in turn, can be used to measure macroscopic flow-velocity and flow-pattern of gas. This measurement method has advantages such as noncontact measurement: no need to add tracing particles which are far larger than molecular volume in the gas flow; no interference with flow field; no limitations to magnitude of flow-velocity and flow-acceleration; being able to conduct simultaneous measurement of multiple points; and being able to obtain parameters, such as gas density, temperature, compositions, etc. simultaneously. It also possesses great potential for measuring various nonhomogeneous gas flows and turbulent flows.

## LITERATURE

- [1] Wolfgang, Demtroder, *Laser Spectroscopy, Basic concepts and Instrumentation*, Spring-Verlag Berlin Heidelberg, New York (1981).
- [2] Gao Zhi, *China Science (A Volume)*, 11 (1984)
- [3] Yeh, Y., cummins, H.E., *Appl. Phys. Lett.*, 4 (1964)
- [4] Sinclair, D.C., Bell, W.E., *Gas Laser Technology* Holt, Rinehart and Winston, Inc. (1969)
- [5] Schlichting, H., *Boundary Layer Theory*. (Fourth Edition), McGRAW-HILL BOOK COMPANY.

DISTRIBUTION LIST  
DISTRIBUTION DIRECT TO RECIPIENT

<u>ORGANIZATION</u>	<u>MICROFICHE</u>
A205 DMAHTC	1
A210 DMAAC	1
B344 DIA/RTS-2C	9
C043 USAMIA	1
C500 TRADOC	1
CS09 BALLISTIC RES LAB	1
CS10 R&T LABS/AVRADCOM	1
CS13 ARRADCOM	1
CS35 AVRADCOM/TSARCOM	1
CS39 TRASANA	1
CS91 FSTC	6
C619 MIA REDSTONE	1
D008 NISC	1
E053 HQ USAF/INET	1
E404 AEDC/DOF	1
E408 AFWL	1
E410 AD/IND	1
E429 SD/IND	1
P005 DOE/ISA/DDI	1
P050 CIA/OCR/ADD/SD	2
AFIT/LDE	1
FTD	1
CCV	1
NSA/PHS	1
LLNL/Code L-389	1
NSA/NST-44	1
NSA/1213/TDL	2
ASD/FTD/TQIA	1

END

3-87

DTIC